Materials and Design 194 (2020) 108916

Contents lists available at ScienceDirect

Materials and Design

journal homepage: www.elsevier.com/locate/matdes

Self-contracting oxidized starch/gelatin hydrogel for noninvasive wound closure and wound healing

Qin Mao [a,b], Oskar Hoffmann [c], Kun Yu [a,b], Fei Lu [a,b], Guangqian Lan [a,b], Fangyin Dai [a,b], Songmin Shang [d,*], Ruiqi Xie [a,b,d,**]

[a] State Key Laboratory of Silkworm Genome Biology, College of Textile and Garment, Southwest University, Chongqing 400715, China
[b] Chongqing Engineering Research Center of Biomaterial Fiber and Modern Textile, Chongqing 400715, China
[c] Department of Pharmacology and Toxicology, University of Vienna, Vienna, Austria
[d] Institute of Textiles and Clothing, The Hong Kong Polytechnic University, Hong Kong

HIGHLIGHTS

- Schiff base structure was introduced as shape memory net-points.
- The transition temperature was around physiological temperature (38 °C).
- Elongated hydrogel could close the incision noninvasively following thermal stimulation.

GRAPHICAL ABSTRACT

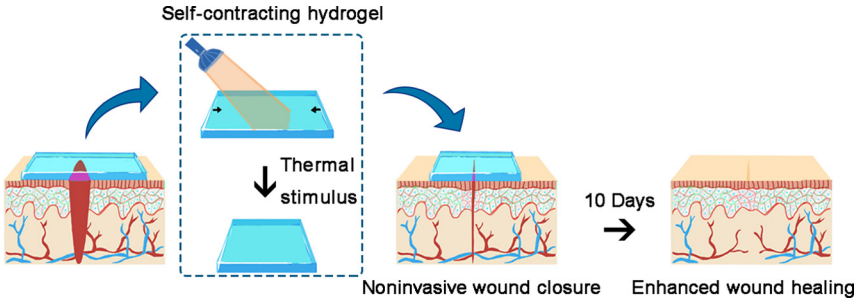

ARTICLE INFO

Article history:
Received 8 May 2020
Received in revised form 19 June 2020
Accepted 21 June 2020
Available online 6 July 2020

Keywords:
Shape memory hydrogel
Gelatin
Noninvasive
Self-contracting
Suture

ABSTRACT

Major challenges in traditional wound closure methods (*e.g.* using sutures and skin staplers) remain inadequately unaddressed; these invasive treatments induce extra puncture wounds, anesthetic side effects, and severe scarring. Herein, an oxidized starch/gelatin-based shape memory hydrogel (OSG) was fabricated as a self-contracting wound dressing to facilitate noninvasive wound closure. The self-contracting properties were attributed by introducing crosslink net-points in the hydrogel polymer structure through Schiff base reaction between oxidized starch (OS) and gelatin. We systematically investigated the self-contracting properties to determine the feasibility of the hydrogel to treat wounds and promote wound closure noninvasively. Following elongation, OSGs could be entirely fixed in a temporary shape at 4 °C, and then contracted under infrared irradiation (IR) for shape memory activation near human physiological temperature (38 °C), providing sufficient recovery force (4 kPa) for successful noninvasive wound closure. Additionally, H&E staining revealed that thicker epidermis and dermis layers were achieved upon OSG treatment, confirming that the OSG facilitated tissue reconstruction in an *in vivo* rabbit model. Moreover, the OSG-treated wounds displayed smoother skin and no visible scarring compared to sutured wounds. Such excellent performance suggests that OSG hydrogel exhibits high potential as an alternative to medical sutures to facilitate noninvasive would closure.

1. Introduction

Considerable research in recent years has been focused on the development of effective suture methods for wound closure owing to the need for timely and effective treatment injuries; accordingly, numerous

* Correspondence to: S. Shang, Institute of Textiles and Clothing, The Hong Kong Polytechnic University, Hong Kong.
** Correspondence to: R. Xie, Chongqing Engineering Research Center of Biomaterial Fiber and Modern Textile, Chongqing 400715, China.
E-mail address: xie.ruiqi@connect.polyu.hk (R. Xie).

https://doi.org/10.1016/j.matdes.2020.108916

and different suture methods and materials have been investigated [1]. Medical wound suture, which has the advantages of high tensile strength, good toughness, and relatively low price, is frequently used for wound stitching along with tissue ligation and fixation. However, the traditional suture method also has several disadvantages as it can be time-consuming, requires professional skills, and, as an invasive treatment, may result in infection and inflammation [2]. A common alternative wound closure method utilizes a skin stapler to connect the wound edges, and can significantly reduce the operative time [3]. However, this method is highly invasive and is associated with a number of drawbacks including pain, high risk of infection, more severe scarring, and difficulty in removal. Recently, noninvasive wound closure devices, such as Zipline™, have been introduced to connect the wound edges without using any medical suture or staple [4]. However, this method may increase the risk of contamination and infection as the wound area is directly exposed to the external environment. Moreover, it is difficult to maintain the moisture content inside the microenvironment of wounds, which has been confirmed by preclinical data to facilitate wound healing [5]. Consequently, multipurpose materials combining suture and wound dressing functionalities are highly needed to facilitate noninvasive wound closure and wound healing.

Recently, shape memory materials (SMMs) have attracted considerable attention in the biomedical field, owing to their multifunctional and stimuli-responsive capacities [6]. As materials that can memorize their original state, SMMs are capable of returning from a deformed state (temporary shape) to the original state (permanent shape) in response to an external stimulus, such as heat, solvent, or light [7–9]. Based on the memory feature of SMMs, numerous studies have been conducted to determine their potential for either wound closure or wound healing applications. Lendlein et al. firstly described a SMM-based suture with self-tightening capacity for wound closure that could shrink and tighten the knot when heated to a temperature above 46 °C [10]. Moreover, Biswas et al. prepared a polyurethane-based body temperature-responsive self-tightening suture. This SMM could be used as an "automatic" suture to close the lips of the wound following shape recovery activation at physiological temperature [11]. Recently, Li et al. investigated a multi-responsive zwitterionic shape memory polymer that could perfectly fit and tightly bind to the wound site following thermo/moisture-induced shape recovery [12]. However, although these smart sutures provided appropriate recovery force to prevent scar tissue and necrosis of the surrounding tissue, they still have to be used as suture materials in an invasive way.

Few studies have been conducted regarding SMM utilization in applications combining noninvasive wound closure and wound healing. SMM-based wound dressings were hypothesized to attach to the contour of the wound skin in an elongated temporary shape, and were demonstrated to contract in response to an external stimulus, thereby closing the wound noninvasively. For the successful development of wound dressings for noninvasive wound closure, some essential properties of SMMs should be considered. Firstly, wound dressings should be capable of controllable shape memory capacity to self-contract wound skin to facilitate wound closure [13]. Secondly, wound dressings should be able to provide proper recovery force, as preclinical data have shown that if the force is too strong or too weak, necrosis of the surrounding tissue or scarring could occur [10]. Lastly, wound dressings should be biocompatible and maintain wettability to facilitate wound healing [14].

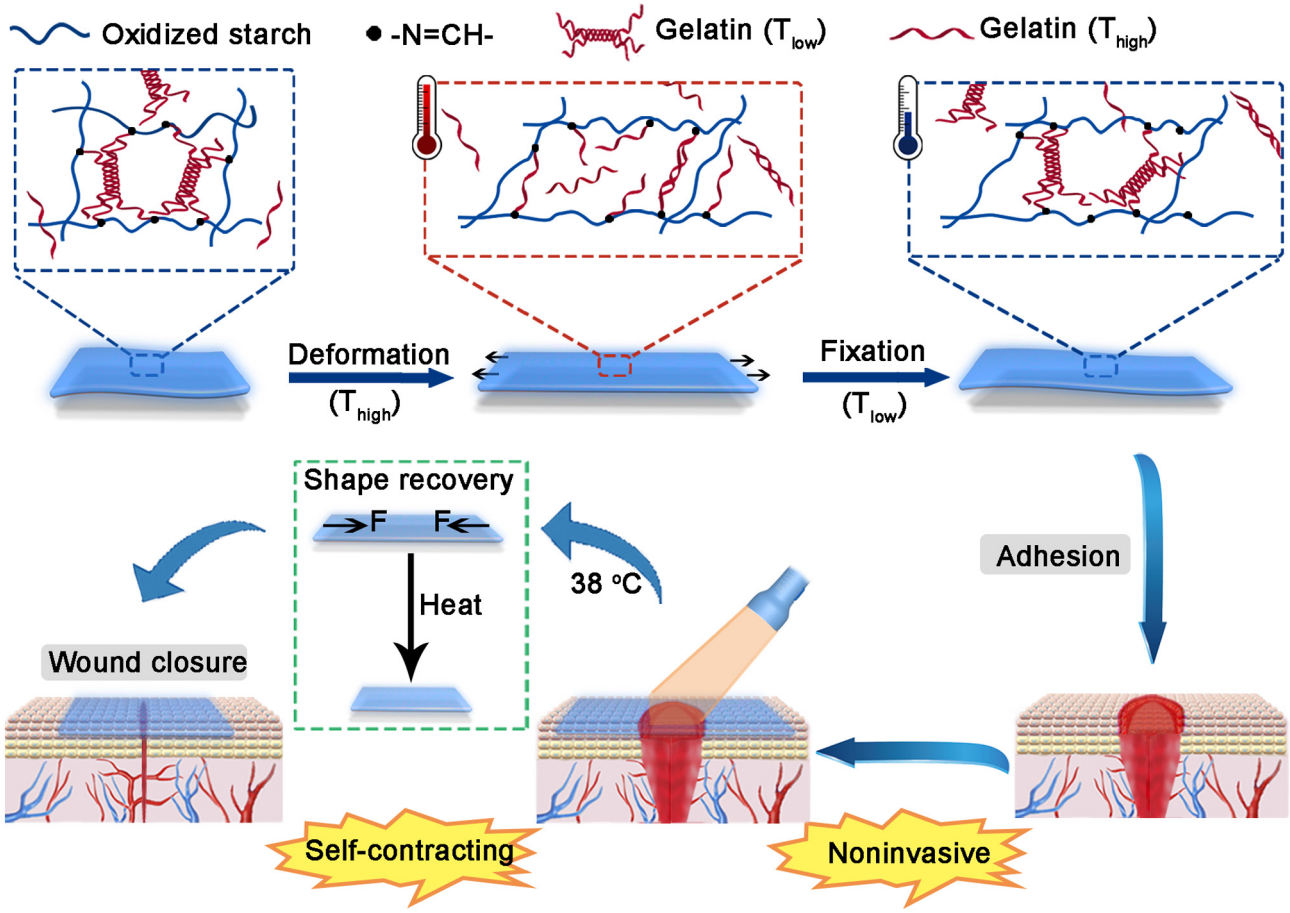

Fig. 1. Schematic representation of self-contracting OSG for noninvasive wound closure and healing.

Gelatin, as an ideal thermo-reversible hydrogel, shows considerable potential in the development of thermo-responsive biomaterials because of its reversible triple helix structure at low temperature [15]. However, gelatin generally exhibits poor mechanical strength and no shape memory capacity, as it lacks stable molecular entanglement as net-points in the polymer structure. Net-points, a necessary functional component in the shape memory polymer network, play a critical role in the shape recovery process [16]. One strategy to endow gelatin with shape memory property is by introducing stable net-points in the gelatin-base polymer structure. For example, we previously generated a thermo-responsive SMM with chemical crosslinks as net-points that exhibited excellent shape memory capacity [17]. Similarly, Zamani Alavijeh et al. synthesized a biodegradable shape memory hydrogel, in which chemical crosslinks were introduced in the polymer network through Schiff base reaction between the amino groups of gelatin and the -N=C=O groups of UPy-hexyl-isocyanate [18]. Therefore, the combination of gelatin and materials containing aldehyde groups could be potentially promising for synthesizing shape memory hydrogels to meet the requirements of smart materials for wound closure and wound healing.

In this study, to facilitate noninvasive wound closure and wound healing, we fabricated an oxidized starch (OS)/gelatin based shape memory hydrogel (OSG). In the OSG, the thermo-reversible gelatin acts as a shape memory switch, and the crosslinks derived from Schiff base reaction between the aldehyde groups of OS and the amino groups of gelatin serve as shape memory net-points. Accordingly, the crosslinked structure could enhance the structural stability and mechanical properties of OSG, which also provided OSG with sufficient shape recovery force after activation. As shown in Fig. 1, when the stretched OSG, whose shape had been fixed temporally, was attached to the wound skin, it allowed the wound lips to close noninvasively by its self-contracting property when stimulated by increasing the temperature over the transition temperature (T_{trans}). Additionally, OSG could also accelerate wound healing, as the moisture content inside the microenvironment of wounds was well maintained [19]. The net-points (chemically cross-linked) of the structure in the shape memory polymer network were carefully investigated. Shape memory effect and self-contracting capacity following shape memory activation were also investigated *in vitro* and *in vivo*. Additionally, in order to examine the capacity of the material to facilitate wound healing, the depths of the cap in the wound sites were also evaluated in detail using a rabbit critical-size incision model. The current study may support the feasibility of noninvasive wound closure using the novel material, and may demonstrate its efficacy in promoting wound healing.

2. Materials and methods

2.1. Materials

Soluble starch was provided by ZhiYuan Chemicals. Co., Ltd. (Tianjin, China). Gelatin (type A from ox bone, 240 g bloom) and sodium periodate ($NaIO_4$) were purchased from Aladdin Chemical Co. Ltd. (Shanghai, China). Sulfuric acid (H_2SO_4) was used to adjust the pH of the solution.

2.2. Synthesis of OS and oxidized starch/gelatin hydrogel (OSG)

The protocol for preparation of OS was adapted from two previously reported methods [20,21]. Firstly, 4.8 wt% of soluble starch solution was prepared by completely dissolving soluble starch in distilled water at 50 °C. Next, the pH of the solution was adjusted to 3.0 with sulfuric acid, then $NaIO_4$ was added to the solution with the ratio of soluble starch and $NaIO_4$ kept at 2:1. The reaction solution was placed in an ice bath and allowed to react for 5 h. Subsequently, the solution was dialyzed against distilled water for four days until the dialysate was free from $NaIO_4$. Before further experimentation, the purified OS was lyophilized 48 h and then milled to obtain the OS powder.

OSG was prepared through Schiff base reaction between OS and gelatin. The OS solution (4.8, 5.6, and 6.4 wt%) was first mixed with the gelatin (20 wt%) solution in a ratio of 9:10 (w/w) at 50 °C; then the mixture was poured into molds and maintained at 50 °C for 1 h until the mixture was solidified.

2.3. Chemical structure determination

The chemical functional groups of OS and OSG were identified using a Fourier transform infrared (FT-IR) spectrometer (Bruker, Daltonics, Germany). The FT-IR spectra were recorded at 4 cm^{-1} resolution in a range of 4000–600 cm^{-1} against a background of KBr and ambient air. A Raman spectrometer (LabRam HR Evolution, Japan) was also used to verify the structure of OS and OSG. The spectra were recorded using an excitation laser of 514 nm and integration time of 10 s.

2.4. Evaluation of the physical properties

The mechanical properties of hydrogels were evaluated using an Autograph AGS-X electronic universal testing machine (Shimadzu, Kyoto, Japan). Rectangular samples ($30 \times 7 \times 2$ mm^3) were tested at the tensile rate of 20 mm min^{-1}. Tensile stress was recorded as a function of strain. According to the stress-strain curves, the stress and elongation at break as well as the Young's modulus were obtained. In addition, the compressive properties of hydrogels (cylinder, diameter = 25 mm, height = 55 mm) were also evaluated at a displacement rate of 1 mm min^{-1} using a compressive plate. The compressive modulus was calculated from the initial linear portion of the slope of the compression curve. The swelling behavior and *in vitro* degradation properties of OSG were also determined by dry weight analysis (Supplementary Method 1 and 2) [22].

2.5. Dynamic rheological test

To obtain the shape memory T_{trans}, dynamic temperature sweeps were performed using a rheometer (Anton Paar, Graz, Austria) to record the changes of storage modulus (G')/loss modulus (G'') of OSG and gelatin as a function of temperature. Samples (cylinder, diameter = 25 mm, height = 1.6 mm) were measured over a temperature range of 4–80 °C at a heating rate of 2 °C min^{-1}, with a constant angular frequency of 10 rad s^{-1} and shear strain of 1%. The temperature at the crossover point of the G' and G'' curve was identified as the T_{trans} of the material. When there was no crossover point, the T_{trans} was identified as the temperature at which G' displayed the maximum slope [18].

The OSG samples with original shape, temporary shape following elongation and fixation, and recovered shape after shape memory activation were prepared for further examination. To monitor the relationship between G'/G'' and shape memory performance of OSG, dynamic rheological measurements of hydrogels were conducted using a strain-controlled (1%) and frequency-controlled (10 rad s^{-1}) mode, respectively (Supplementary Method 3). The thermo-responsive behavior of OSG was also tested using thermo-cycles to identify the recovery force (Supplementary Method 4). Silicone oil was used to spread on the side of the cylinder sample to prevent dehydration during the rheological measurements [23]. Each rheological measurement was performed in triplicate.

2.6. Shape memory behavior

Firstly, the samples ($46 \times 7 \times 2$ mm^3) were stretched to a temporary shape, which was then fixed when cooling to 4 °C. After unloading the external stretching force, the samples were heated to a temperature above 38 °C to activate shape recovery, which was typically in the

range of 38–41 °C. The length of the samples was recorded during the process.

The shape fixity (R_f) and shape recovery ratio (R_r) were calculated using Eqs. (1) and (2) [12].

$$\text{Shape fixity } (R_f) = \frac{L_3 - L_1}{L_2 - L_1} \times 100 \quad (1)$$

$$\text{Shape recovery } (R_r) = \frac{L_3 - L_4}{L_3 - L_1} \times 100 \quad (2)$$

where, L_1 L_2, L_3, L_4 represent the initial length of the sample, the length after stretching, the length after releasing the stress at 4 °C, and the recovered length at $T > 38$ °C, respectively.

Shape recovery force was evaluated through relatively complex thermo-mechanical cycles using strain-temperature control mode ($dT/dt = 2$ °C min^{-1}) on an electronic universal testing machine (Shimadzu Autograph AGS-X). The equipment enables control of the strain and temperature, with the temperature being controlled by switching the heating or cooling devices on or off. This experiment mainly focused on the recovery force evolving upon constrained heating. The experiments involved two stages, in which the rectangular OSG samples ($20 \times 7 \times 2$ mm^3) were: (i) stretched to 50% strain at a rate of 5 mm min^{-1} at 38 °C; and (ii) four thermo-cycles with constant elongation. Each thermo-cycle consisted of a cooling and heating process: firstly, the temperature was cooled to 4 °C and maintained for 10 min; secondly, the sample was heated while the strain was kept constant to generate the recovery stress for 10 min. The shape recovering stresses were recorded as a function of time for further analysis.

In addition, Masson's trichrome staining was used to demonstrate the polymer cluster orientation of OSG during the elongation and recovering process. The OSG hydrogels with original shape, fixed temporary shape (100% elongation), and recovered shape were prepared into cuboids ($10 \times 7 \times 2$ mm^3). Pristine gelatin hydrogels with original and stretched shape (20% elongation) were also prepared as controls for the same Masson's trichrome staining procedure [24]. All samples were obtained using the freezing sectioning method, in which the frozen 6-μm transverse sections were cut along the tensile direction for further staining. Photomicrographs were obtained using a ZEISS microscope.

The pore structure changes prior to and following shape memory activation were determined using a scanning electron microscope (SEM). The OSG samples with original shape, temporary shape, and recovery shape were lyophilized and then immersed in liquid nitrogen to obtain transverse sections. Images of the transverse sectioned OSG hydrogels were obtained using a JSM-6610 SEM (Shimadzu).

2.7. Cytotoxicity assays in vitro

Mouse skin fibroblasts (L929, Chinese Academy of Sciences Cell Bank, Beijing, China) were used to detect the cytotoxicity of OSG hydrogels *via* MTT and live/dead cell staining assays according to ISO standard 10993-5 (Supplemental Method 5).

2.8. Surgical procedure and histological analysis

OSG ($30 \times 30 \times 3$ mm^3) was prepared for animal testing. Initially, 12 New Zealand white rabbits (2–4 months old, approximately 2.0 kg in body weight) were anesthetized with 0.5 ml of xylazine and ketamine hydrochloride. After shaving and sterilizing the surgical areas, three full-thickness incisions were created on the dorsal skin of each rabbit. Then, the OSG hydrogel was adhered around the incision using bioglue in a temporary shape after elongation and fixation. Subsequently, shape recovery of the elongated OSG was triggered by infrared light to control the temperature at 38 °C. Rabbits were housed individually in cages at room temperature to prevent other damage to the wounds and materials. Eventually, rabbits from each group ($n = 4$) were humanely euthanized at 3, 7, or 10 days after surgery for subsequent examinations. Two control groups including rabbits with incisions left untreated and incisions treated with medical suture were also established in the same surgery procedures. The condition of the wound area was recorded using a digital camera, and the wound area was then calculated with ImageJ software. All animal experiments were approved by the Southwest University Animal Care and Ethics committee.

Tissue specimens were collected by removing the skin containing the entire wound and adjacent normal skin. Subsequently, the specimens were fixed with 10% formalin and embedded in paraffin, then sections (5 μm) were cut vertically to the incision and stained with hematoxylin-eosin (H&E) for subsequent histological observations [25].

2.9. Statistical analysis

Statistical analysis was determined using one-way ANOVA. In all cases, differences were considered significant when the probability value (p) < 0.05.

3. Results and discussion

3.1. Structure conformation of the shape memory hydrogel

A strategy for gelatin to obtain shape memory properties at physiological temperature involves introducing net-points to its polymer network, which is expected to be provided *via* Schiff base reaction between the amino groups of gelatin and aldehyde groups of OS (Fig. 2A). As shown in Fig. 2B, pristine OS and gelatin solutions were in the fluid state at 38 °C, while the OSG was in the solid gel state after crosslinking. This figure clearly shows that the OSG hydrogel was formed by the chemical crosslinking of gelatin and OS through Schiff base reaction. The molecular structure of the prepared hydrogel was compared with its pristine raw materials using FT-IR and Raman spectra analysis. Firstly, the appearance of an obviously new stretching vibration band of -C=O at 1738 cm^{-1} in the FT-IR spectrum (Fig. 2C) suggests OS was successfully synthesized. The Raman spectra also confirmed the existence of -C=O in the OS structure (Fig. 2D). There was an obvious peak located in the range of 1717 to 1748 cm^{-1}, which can be assigned to the -C=O group [26]. These results confirmed that the pristine starch has been successfully oxidized by $NaIO_4$.

The self-contracting capacity is attributed to the excellent shape memory of the polymer structure, where the net-points could be inserted *via* Schiff base reaction. In Fig. 2C, the new characteristic band at 1661 cm^{-1} in the FT-IR spectrum can be assigned to the absorption of Schiff base bond (-C=N), which was also confirmed by the presence of the characteristic absorption of -C=N at 1591 cm^{-1} in the Raman spectrum (Fig. 2D) [27,28]. Notably, according to Fig. 2C, the absorption peaks of the amide I and amide II shifted to lower wavenumbers (from 1655 to 1634 cm^{-1}, and from 1552 to 1547 cm^{-1}, respectively) in the FT-IR spectrum of OSG when compared to those of gelatin, indicating that the nucleophile substitution reaction occurred, which resulted in the formation of -C=N groups in OSG. These results suggest that the -C=N structures were successfully introduced into the OSG polymer network, serving as the shape memory net-points.

The equilibrium swelling behavior of the hydrogels was also measured to evaluate the changes in crosslink density in OSG with different concentration of OS. It is known that the equilibrium swelling ratio decreases with the increase of crosslink density in the system. In Fig. 2F, OSG-b exhibited the lowest equilibrium swelling ratio compared to that of OSG-a and OSG-c, suggesting that OSG-b likely possessed the highest effective crosslinking points. The hydrogel possessed higher effective crosslinking points, indicative of less network space between polymer chains, and thus resulting in a lower swelling ratio. Similar results were previously reported for the chitosan/oxidized starch/silica system [29]. Considering these results, the degradation characteristics

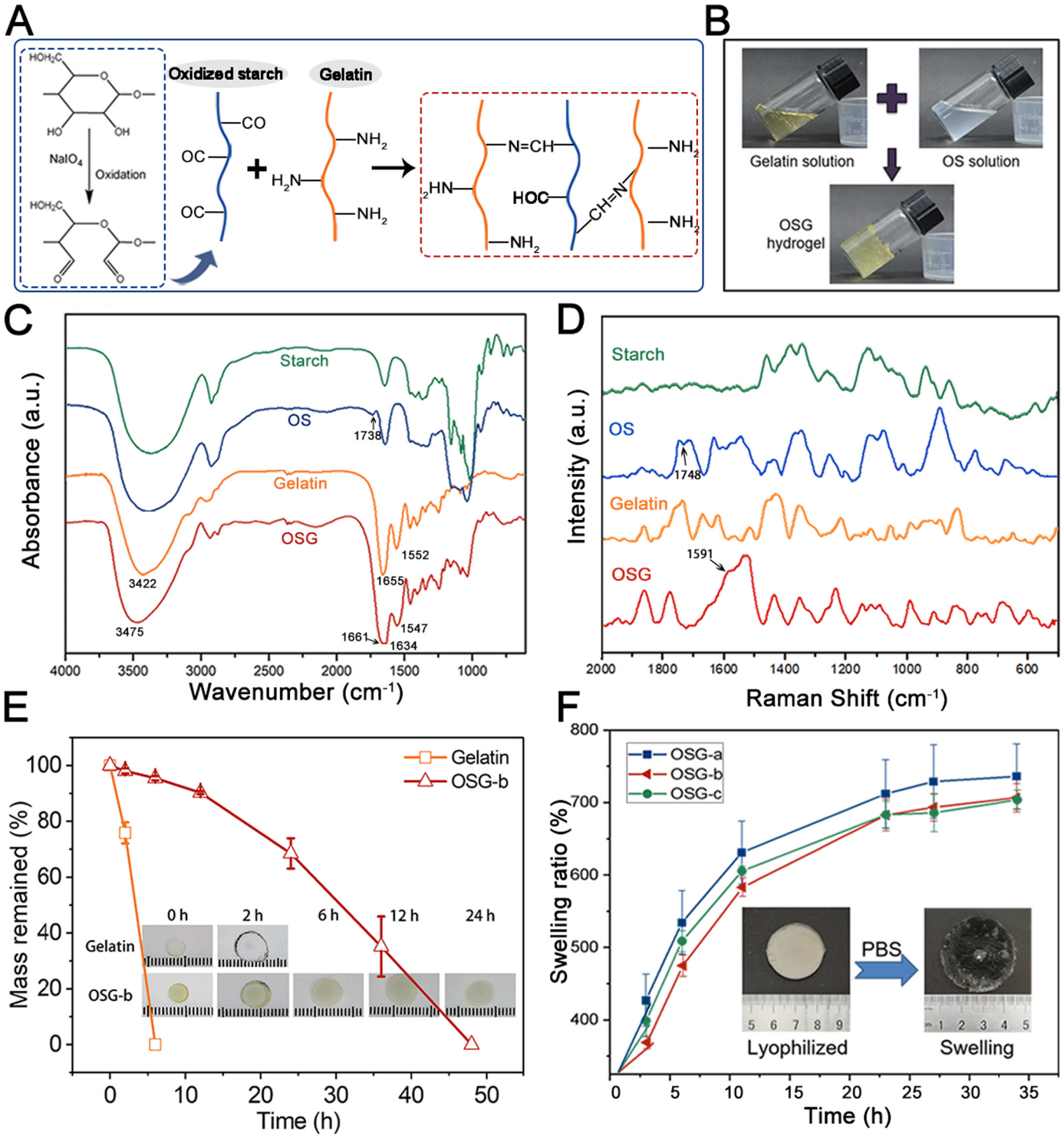

Fig. 2. Chemical structure and characterizations of OS and OSG. (A) Schematic representation of OSG hydrogel synthesis. (B) Photographs of pristine gelatin solution, OS solution prior to crosslinking, and OSG hydrogel at 38 °C. (C) FT-IR spectra and (D) Raman scattering spectra of pristine starch, OS, pristine gelatin, and OSG. (E) Mass retention during degradation of OSG-b and gelatin. (F) Swelling property of OSG hydrogels with different concentration of OS after swelling in PBS at room temperature (OSG-a, b, c including OS of 4.8, 5.6, and 6.4 wt%, respectively). Error bar indicates standard deviation (s.d.) ($n = 3$).

of OSG-b were investigated by weight analysis. As displayed in Fig. 2E, the degradation rate was substantially decreased with the addition of OS, with the complete degradation occurring in <6 h in the case of gelatin and in 48 h in the case of OSG-b, which may be due to the formation of a highly crosslinked polymer network through Schiff base reaction between OS and gelatin.

3.2. Mechanical properties

For successful noninvasive self-contracting application, it is necessary to design a wound dressing material with desirable mechanical properties. The concentration of OS affects the crosslink density of hydrogels, which further influences their mechanical properties. In

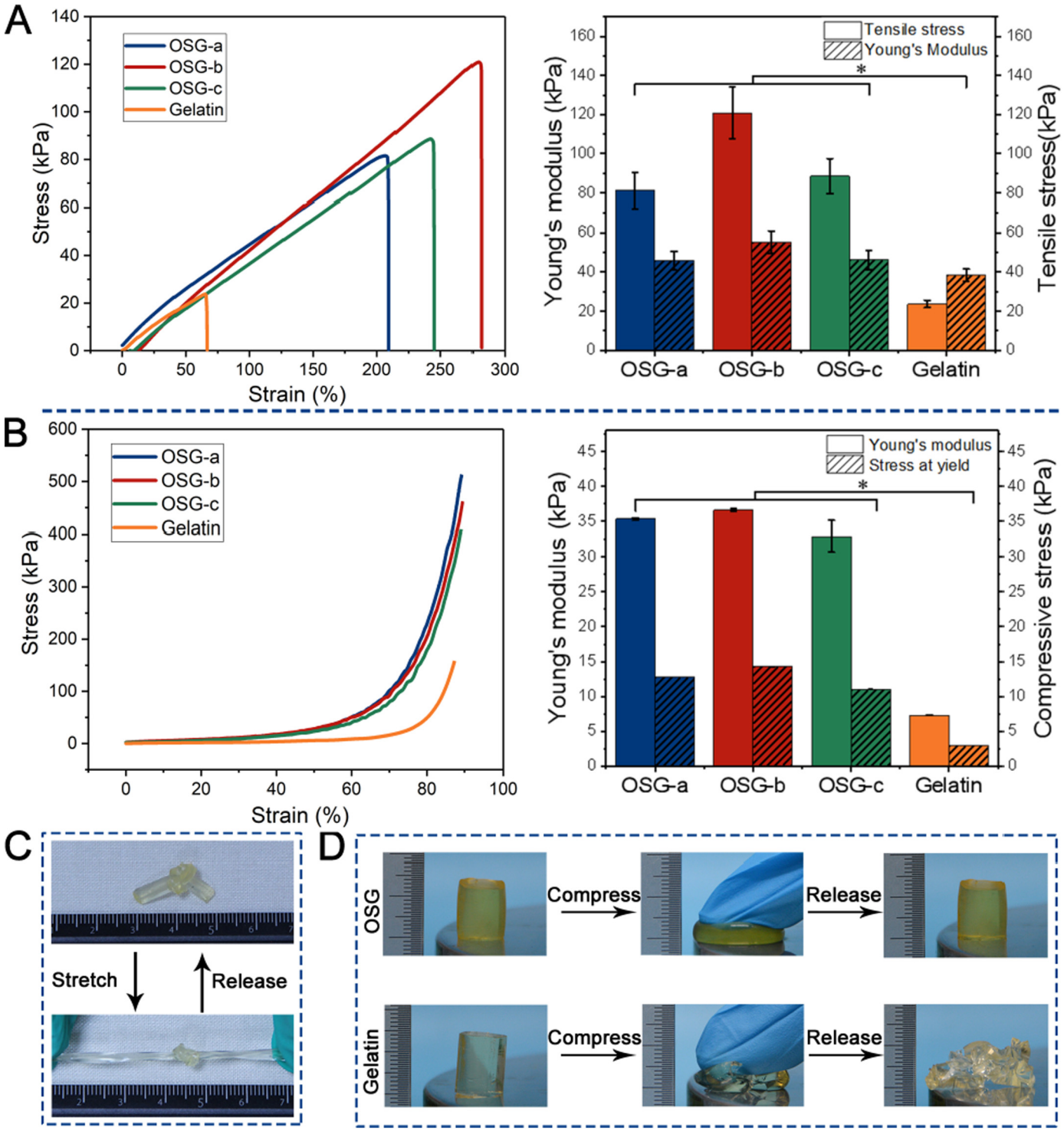

Fig. 3. Mechanical properties of OSG and pristine gelatin. (A) Tensile properties of OSG with different OS concentration and pristine gelatin. Tensile stress-strain curves (left); the calculated tensile stress and Young's modulus (right). (B) Compressive properties of OSG with different OS concentration and pristine gelatin. Compressive stress-strain curves (left); the calculated compressive stress and Young's modulus (right). (C) Photographs of a knotted and twisted OSG sample after stretching and releasing. OSG-a, -b, -c represent OSG with OS concentration of 4.8, 5.6, and 6.4 wt%, respectively. (D) Photographs of the hand-compression and release process applied to OSG and pristine gelatin cylindrical hydrogels. Error bars indicate s.d. (n = 3).

Fig. 3A, the pristine gelatin exhibited maximum elongation of 65% and tensile stress of 23.7 kPa, whereas OSG-b demonstrated maximum elongation of 279% and tensile stress of 120 kPa, almost 4- and 5-fold increases, respectively. A rising trend was observed in the compressive capacity, for which OSG exhibited an increase from 7.3 to 36.6 kPa in Young's modulus and from 2.99 to 14.28 kPa in compressive stress at yield (Fig. 3B). The mechanical strength of OSG initially increased with the addition of OS, and then decreased when an excess of OS was present in the OSG system (OSG-c). This might possibly be explained by the fact that the free amino groups in gelatin rapidly reacted with different OS in the case of high OS concentration, guiding the reaction in an early stage towards the direction of grafting [30]. It has been shown that the modulus of hydrogel dressings should be consistent with that of the tissues neighboring the wound to ensure the integrity of the wound

dressing during the process of wound healing [31]. In the present study, the tensile Young's modulus values of OSG hydrogels were 45–55 kPa, which were comparable to those of human skin (23–101 kPa) [32].

According to Fig. 3C, the OSG could also be knotted and twisted without fracture, suggesting that the hydrogel retained robust mechanical properties and excellent resilience. Fig. 3D also illustrates that the OSG hydrogel could restore rapidly after compression, whereas the pristine gelatin hydrogel was easily fractured. This might derive from the chemical crosslinked structure in the OSG system, which enhanced the mechanical properties and thus may facilitate its application for wound closure.

3.3. Rheological characteristics

To investigate the shape memory mechanism of OSG hydrogel, dynamic rheology tests were performed to evaluate its thermodynamic properties and T_{trans}. Fig. 4A shows that OSG hydrogels exhibited higher G' than G'' value in the range of the linear viscoelastic region, suggesting that the hydrogel in all states constituted a typical gel-like system with behavior likely comparable to that of an elastic solid [8]. After the intersection point (gel point) between G' and G'', the hydrogel exhibited a fluid-like state with a collapsed network [33]. The shear strain at the gel point was decreased from 142% to 71% following OSG deformation and fixation at the temporary shape. This might be explained by the fact that the OSG at the temporary state was elongated before testing, allowing easier disruption of the polymer aggregates in the hydrogel [26]. It is also worth noting that G' of recovered and temporary samples is slightly weaker than that of original sample in the linear region, which might be ascribed to the fact that the temporary and recovered samples remove the residual stress that originates from processing. Moreover, this confirmed the function of net-points in the shape memory polymer network. The permanent shape of the shape memory network was stabilized by covalent net-points, which allowed OSG to spontaneously recover its permanent shape following shape memory activation because of the entropy relaxation of the material [34].

Fig. 4B shows the G' and G'' curves of the OSG hydrogels as a function of angular frequency at room temperature. For all OSG hydrogels, the G' value was considerably higher than the G'' value between 1 and 100 rad s^{-1}, and G' showed a marked frequency-independent plateau, which indicated the stable structure of the gel network. These results suggest that the hydrogels in original, temporary, and recovered states had a well-developed network possessing good long-term stability and high mechanical strength [8].

The T_{trans} of OSG hydrogels was measured by using the dynamic viscoelastic method. The G' and G'' at constant strain amplitude (1%) and angular frequency (10 rad s^{-1}) were measured as a function of temperature. In Fig. 4C, the typical characteristics of G' and G'' curves can be divided into three segments: a slight flat region with G' and G'' curves that decreased as the temperature increased; a region with a steep negative slope; and a nearly flat segment. Gelatin forms a physical network at low temperature, whereas the physical network of pristine gelatin is not stable at body temperature. In Fig. 4C on the left, the intersection point of the G' and G'' values was located at 36 °C, suggesting the collapse of the physical network of pristine gelatin when heated above 36 °C. In Fig. 4C on the right, the G' value of OSG was higher than the G'' value in the whole temperature range (4–80 °C), indicating that a strong crosslinked structure was obtained in the OSG hydrogel. Moreover, the viscoelastic modulus had the largest incline at 38 °C, which was defined as the T_{trans} of OSG [18].

Dynamic rheological testing was further employed to clarify the shape memory behavior of the OSG hydrogels. As it can be seen in Fig. 4E, the G' difference ($\Delta G'$) between the original and temporary samples was significantly higher at 40 °C than that at 20 °C, indicating that more stored energy was released after shape memory activation above the T_{trans} (38 °C) for the temporary OSG. G' indicates that the stress energy is temporarily stored but can be recovered afterward [35]. Because of the deformation/elongation process occurring during the preparation of OSG in the temporary state, this sample restored more energy following shape fixation. The restored energy was fully released, corresponding to the decrease of G' following shape memory activation above the T_{trans}. In addition, there was no significant difference between the G' of the temporary state and that of the original state at 10 °C in the last cycle. This suggests that the G' value at 10 °C could almost return to the original value after shape recovery induction at 40 °C, reflecting that the rheological structure was almost fully recovered compared to that of OSG in its original state [32]. In addition, the tanδ of both OSG and gelatin raised to the highest values at 38 °C during temperature sweep from 20 to 80 °C (Fig. S4), implying that the increase in tanδ of OSG might be attributable to the thermo-responsive gelatin component. In comparison with the considerable tanδ increase in gelatin (to higher than 1000), the tanδ of OSG was always lower than 1 during the temperature sweep, indicating that the chemical network in OSG, resulting from the Schiff base reaction, retains its structure regardless of the temperature. These results demonstrate that the chemical crosslinked net-points and thermo-responsive gelatin components endowed shape-memory capability to the OSG hydrogel [36].

3.4. Shape memory behavior

Masson's trichrome staining is frequently used for the detection of collagen fibers, following the general rule that less porous tissues are colored by the smallest dye molecule followed by the larger molecule [37]. In particular, a previous study concluded that the differences in the penetration, retention, and displacement of arylmethane dyes could lead to the red staining of collagen/gelatin, in which more positively charged amino dye-binding sites are available [38]. In the present study, Masson's trichrome staining was used to stain the gelatin-based hydrogels to detect the changes in orientation of the substrate material during the shape recovery process. As shown in Fig. 5A, the gelatin-based substrate (dark color) in the original shape presented an approximately isotropic arrangement. After stretching and fixation with concomitant loss of entropy, the macromolecular cluster of temporary OSG exhibited obvious orientation along the force direction, presenting a parallel orientation. Following shape memory activation, the re-arrangement of the polymer network structure returned to the corresponding original state characterized by the isotropic structure of the base material, during which the materials gained back the previously lost entropy. In comparison, no obvious changes were observed prior to or following shape memory deformation and fixation in the pristine gelatin hydrogel. Thus, these results suggest that the shape memory capacity could be attributed to the entropic elasticity at the molecular scale [34].

The pristine gelatin hydrogel had no shape memory property, as there were no stable physical crosslinks as net-points at higher temperature in its polymer structure. Generally, there are two methods to provide such thermally stable net-points: increasing the molecular weight to form thermally stable physical crosslinks or introducing a chemical crosslinker to form stable chemical crosslinks [39]. In the present case, OS was introduced as a chemical crosslinker to form a thermo-responsive gelatin-based network. As shown in Fig. 5B, OSG exhibited effective shape memory fixation ($R_f = 94.7\%$) at 4 °C and shape recovery ($R_r = 95.5\%$) upon triggering shape memory at 38 °C for approximately 30 s. SEM showed the pore structure of OSG hydrogels, in which the mean pore size was 150 μm. OSG could be fixed in an elongated shape, exhibiting aligned narrow pore architecture along the stress-loading orientation. After reheating above 38 °C to activate shape recovery, the pore structure recovered to the original state. The results demonstrate that the micropore structure of the OSG hydrogel was not damaged during the shape deformation and recovery processes, which supports the feasibility of OSG use in wound closure and wound healing applications.

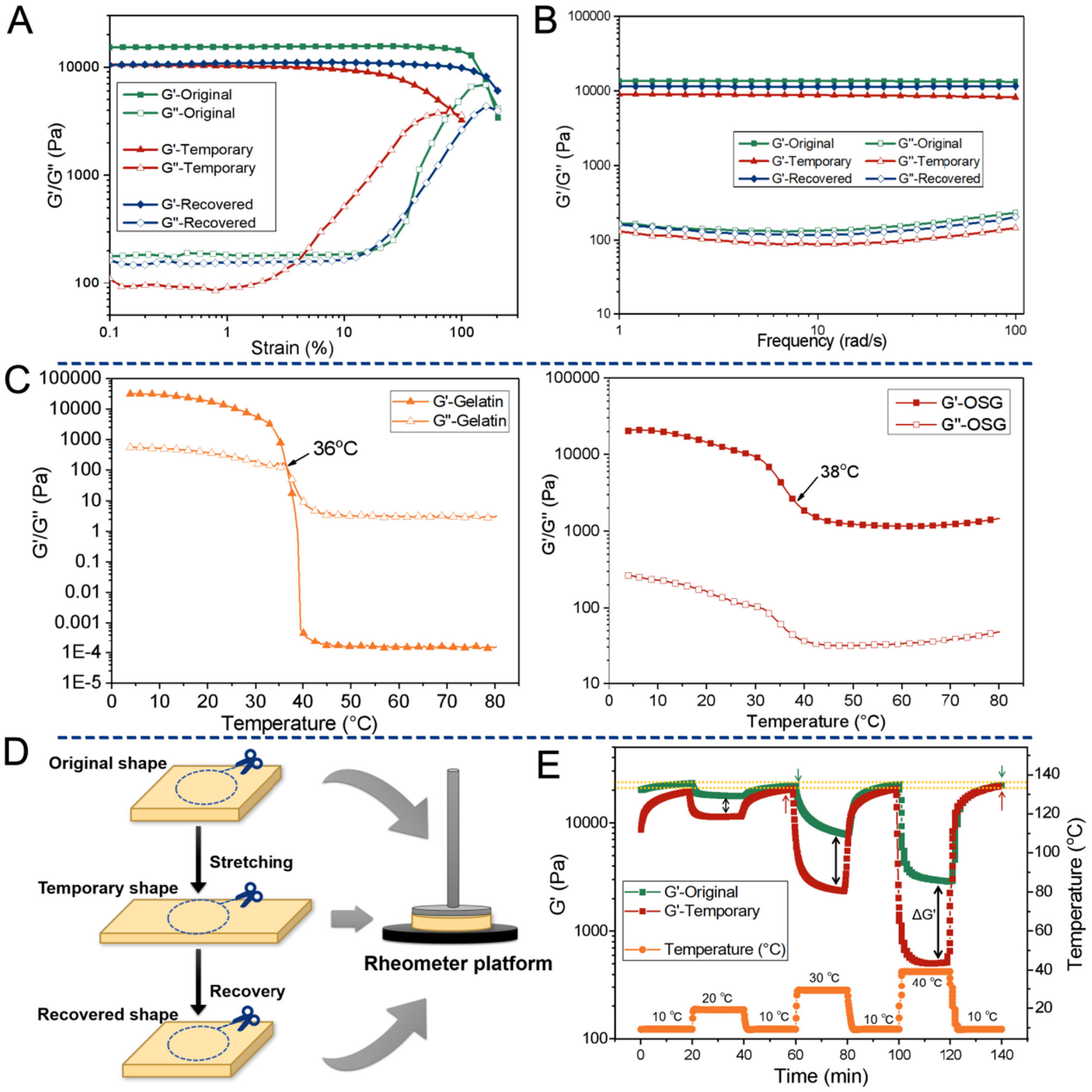

Fig. 4. Rheological properties of OSG. (A, B) Storage modulus and the loss modulus as a function of strain (A) and frequency (B) of OSG in original shape, temporary shape, and recovery shape. (C) Temperature-dependent changes of the storage modulus (G') and the loss modulus (G'') of pristine gelatin (left) and the OSG-b (right). (D) Schematic of sample preparation for rheological tests. (E) Time-dependent changes of the storage modulus for OSG in original shape and temporary shape in three isothermal sweep cycles.

A thermo-mechanical cycle test under strain control mode was performed to exam the recovery force of OSG hydrogel and inspect the repeatability of the shape memory capability (Fig. 5C). OSG was elongated by 50%, and then cooled for a short period of time to 4 °C. With constant elongation, the recovery force (approximately 4 kPa) was generated correspondingly after increasing the temperature to T_{trans} (38 °C), which was contributed by the stored energy release. During the entire thermo-mechanical cycle test, obvious downward slants in stress could be observed, which might be associated with the stress relaxation under constant elongation control. Notably, the stress relaxation did not differ significantly from the recovery force generated in all thermo-mechanical cycles, suggesting good repeatability of the recovery force generated. These results corroborate the added value of the OSG self-contracting capacity in wound closure applications.

3.5. Self-contracting capacity and noninvasive wound closure performance in vivo

Before assessing the self-contracting capacity of the OSG hydrogel *in vivo*, *in vitro* cell biocompatibility was determined by cell viability

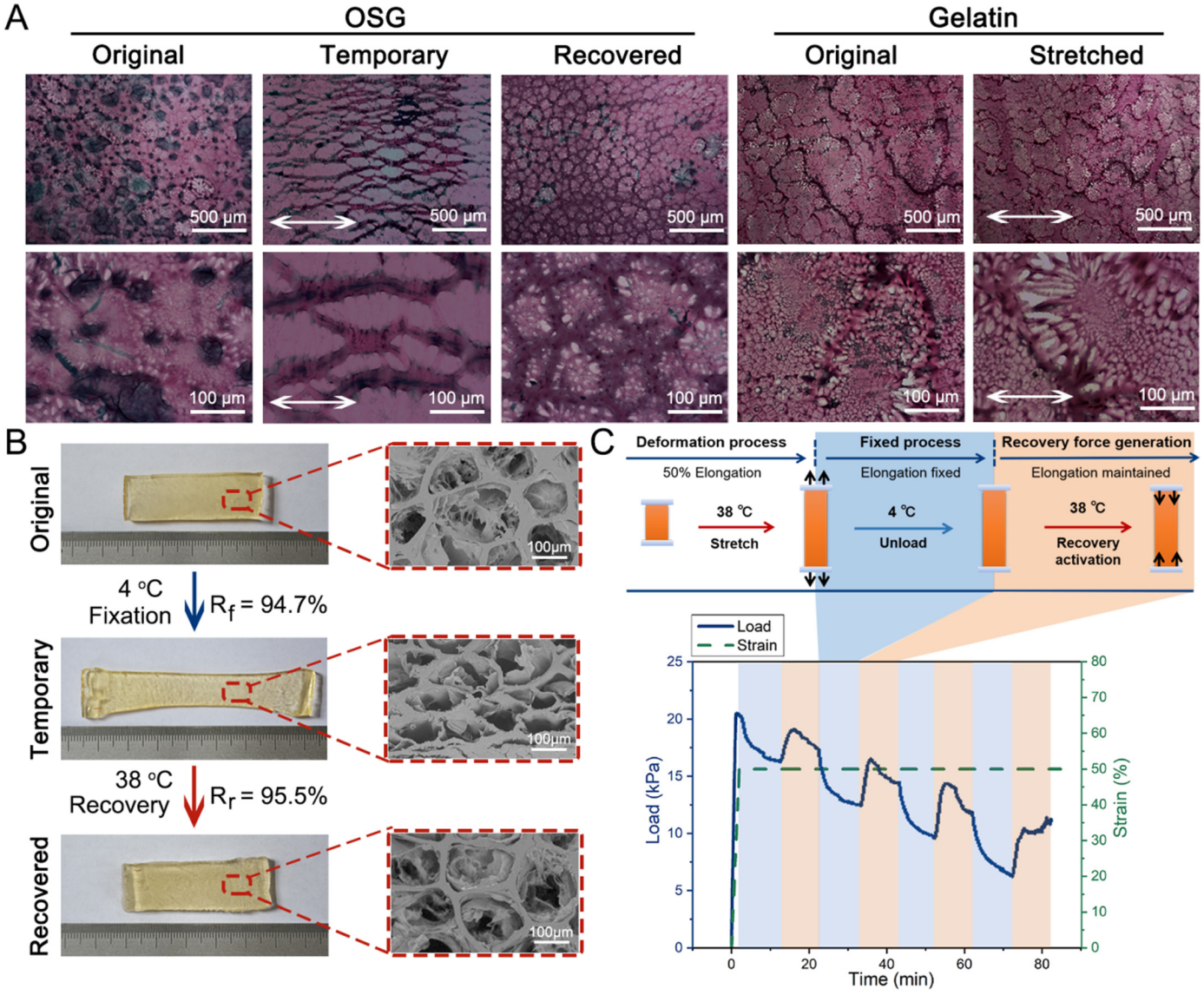

Fig. 5. Shape memory properties of OSG. (A) Masson's trichrome staining of OSG (in original, temporary, and recovered shape) and gelatin hydrogel (in original and stretched shape; the recovered shape of gelation is not presented because pristine gelatin has no shape memory capacity). The arrows represent the tensile orientation. (B) Photographs of the OSG sample and SEM of the boxed sections in original, temporary, and recovered states. (C) Shape recovery force determination with a strain control mode in four thermo-mechanical cycles.

and live/dead staining. The results show that OSGs with different OS concentrations exhibited good biocompatibility (Supplementary Fig. S3). The self-contracting capacity of the OSG was investigated using the dorsal full-thickness incision model. As can be seen in Fig. 6A, the OSG hydrogel after elongation and fixation was initially adhered to the rabbit skin around the incision site. After triggering at 38 °C, the OSG rapidly contracted from the elongated shape and pulled the skin around the incision to close the wound. In addition, Supplementary video 1 is provided to better demonstrate the self-contracting capacity of OSG for wound closure. The successful closure of the wound suggested that the OSG hydrogel provided sufficient recovery force for wound closure in a non-invasive manner.

3.6. Wound healing capacity in vivo

Wound closure and healing processes were monitored over time *in vivo* as shown in Fig. 6B and C. The OSG and medical suture groups displayed faster wound healing than the blank control group without any treatment. The healing process was slower and more scar tissue was produced in the blank control group compared to the other groups. Owing to the lack of external force to promote wound closure, the wound healing in the blank group was fully reliant on the migration of cells from surrounding tissues [2]. Moreover, the usage of OSG hydrogel, which does not require professional skills, significantly expedited the operation procedure in comparison to conventional surgical suturing. The wound treated with OSG after 10 days exhibited a visually smaller wound area compared to that of the blank control group, being even slightly smaller than that of the medical suture group. Notably, although the suture served to close the wound, it had the potential to cause secondary damage upon removal at day 7, leading to incomplete wound closure. Furthermore, it is interesting to note that the wound treated with OSG displayed smoother skin and no obvious scar formation compared to that treated with suture and Mepiform® dressing at day 10 after surgery. One possible reason might be that the OSG distributes stress more evenly and provides uniform closure across the incision, whereas stitching by suture induces stress on specific points where the skin is punctured. Moreover, the self-contracting and wound closing capacities might also take effect. OSG hydrogel, as against Mepiform®

dressing, could provide a more evenly distributed (and hence, more favorable) stress environment to enable the wound to close completely. Thus, the OSG hydrogel displayed high shape recovery efficiency and demonstrated strong potential as an effective alternative to medical sutures for noninvasive wound closure and subsequent wound healing.

3.7. Histological analysis

H&E staining was performed to evaluate the overall wound healing capacity of OSG. Generally, normal skin can be divided into three layers including epidermis, dermis, and hypodermis [39]. As demonstrated in Fig. 7A, the OSG group showed significant granulation tissue and light inflammation at day 3 post-surgery. At day 10 post-surgery, more complete epidermal and dermal structures along with greater detachment of the callus from the epidermis was observed in both suture and OSG groups, whereas obvious structural disorders of the wound sites were visible in the blank control group, which received no treatment. The results illustrate that OSG facilitated granulation tissue formation and re-epithelialization of the wounds. Moreover, 10 days after surgery, an obvious 2.0-mm-depth gap remained in the blank control group, whereas the depth of the gap in the OSG-treated group had decreased dramatically from 2.0 mm to 0.5 mm (Fig. 7C). This result suggests that the OSG-sealed skin incision was successfully healed. OSG also exhibited superior wound healing capacity in comparison to that of the

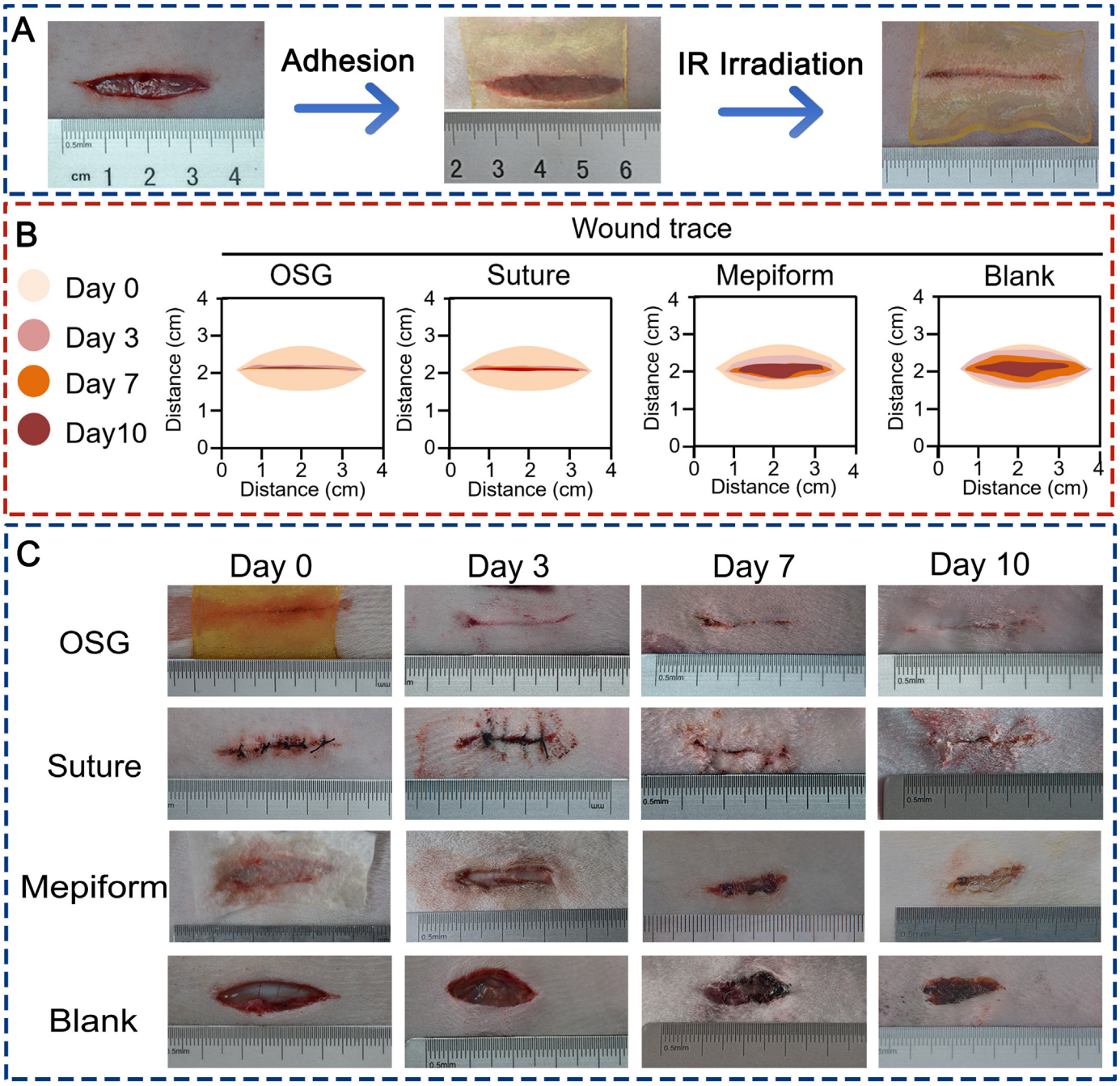

Fig. 6. (A) Noninvasive wound closure effect of self-contracting OSG applied on a dorsal full-thickness incision model. Wound healing effect of different wound closure methods. (B) Schematic of wound area traces on different days (day 0, 3, 7, and 10) after surgery. (C) Photographs of the wounds either untreated or treated with OSG hydrogel or medical suture. OSG was removed before photographing at day 3, 7 and 10 post-surgery.

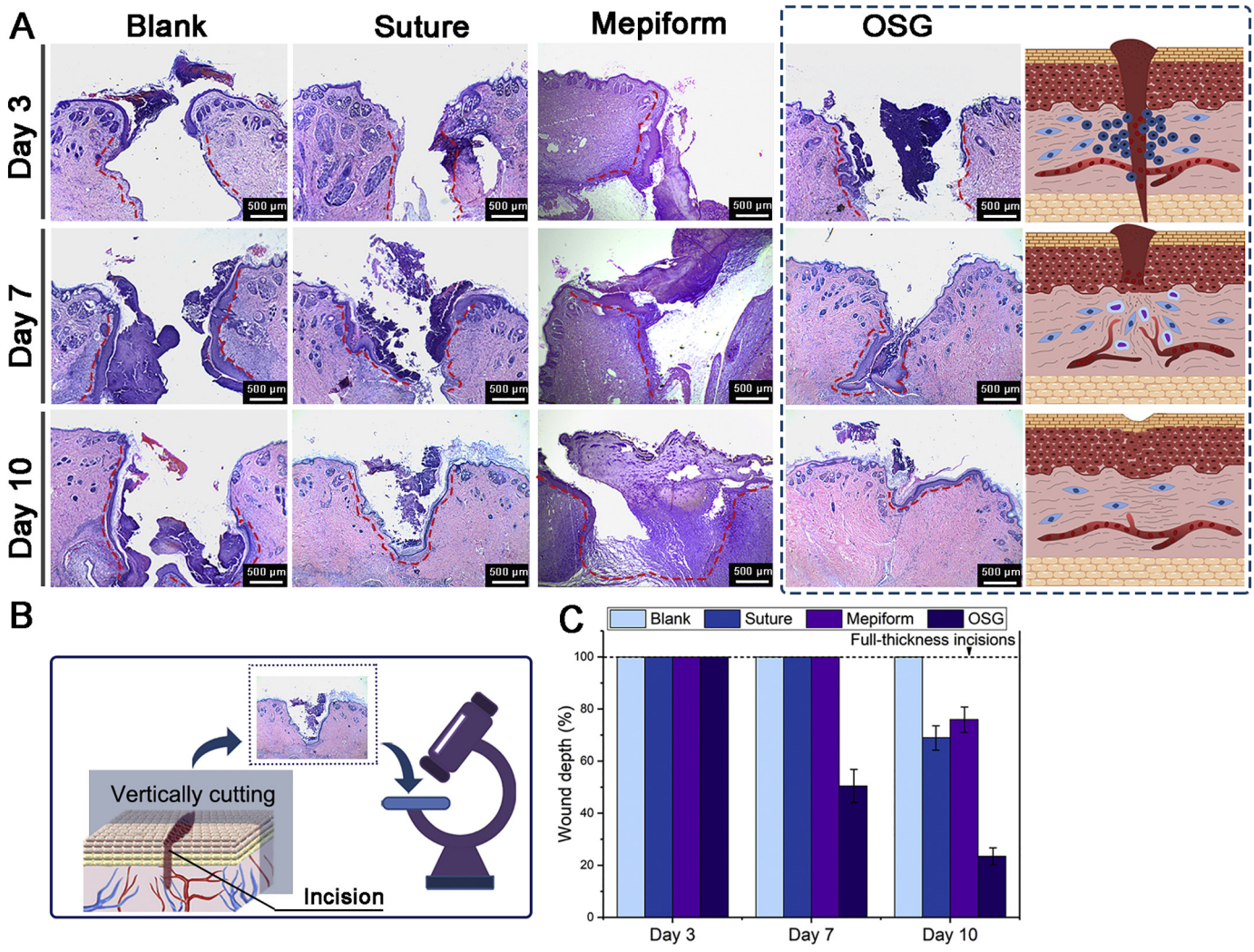

Fig. 7. Histological evaluation of wound healing. (A) Histological analysis using H&E staining. The wound area is labeled with red dashed lines; the inflammation areas are indicated with yellow arrows. (B) Schematic of the sampling of sections. (C) Wound depth of the three groups 3, 7, and 10 days after surgery. Error bars indicate s.d. (n = 4).

suture and Mepiform® dressing, as evidenced by the respective gaps with depths of approximately 1.4 mm. In addition, levels of inflammation with various treatments were assessed by a score system (Fig. S4). At day 3 post-surgery, all groups exhibited similar levels of inflammation and no severe immune response. This result, in agreement with the cytotoxicity determination (Fig. S3), is indicative of good biocompatibility. However, greater numbers of inflammatory cells in blank control and suture group compared with that in the OSG group at day 7 post-surgery. This might be attributable to the fact that the OSG facilitated wound closure and promoted/accelerated the wound healing [40]. Apart from the effective wound healing capacity, these findings also indicate that OSG might be superior to suture with regard to 1) the feasibility of noninvasive wound closure; 2) the effect of reducing wound inflammation degree; and 3) no professional skill requirement for wound closure.

4. Conclusion

In summary, to endow gelatin shape memory capacity, OSG was successfully produced through the introduction of Schiff base (-N= C) constructs as net-points in the polymer structure. As a result of the successful introduction of shape memory net-points, the OSG exhibited an effective thermo-responsive shape memory property with T_{trans} (38 °C) near physiological temperature. Orientation of macromolecular clusters was further identified prior to and following shape memory activation, changing from parallel orientation to random coil, during which the materials gained back the entropy lost in the deformation step. In addition, the OSG hydrogel exhibited sufficient mechanical capacity and tissue compatibility for wound healing and facilitated wound tissue remodeling. The OSG wound dressing could self-contract the attached skin from the elongated shape to close the incision noninvasively following thermal stimulation. Histological analysis further demonstrated the occurrence of successful wound repair. Thus, OSG is an attractive alternative to sutures, and is a multifunctional wound dressing for noninvasive wound closure that facilitates wound healing. However, more research is necessary to improve the properties of this dressing. The design of self-adhesive substances, for instance, is essential to endow the material self-adhesion to skin and therefore extend the application of SMMs as suture alternatives for noninvasive wound closure.

Supplementary data to this article can be found online at https://doi.org/10.1016/j.matdes.2020.108916.

CRediT authorship contribution statement

Qin Mao: Investigation, Formal analysis, Writing - original draft. **Oskar Hoffmann:** Writing - review & editing. **Kun Yu:** Formal analysis. **Fei Lu:** Formal analysis. **Guangqian Lan:** Formal analysis. **Fangyin Dai:** Formal analysis. **Songmin Shang:** Validation, Writing - review & editing. **Ruiqi Xie:** Validation, Writing - review & editing.

Declaration of competing interest

The authors declared that they do not have any commercial or associative interest that represents a conflict of interest in connection with the work submitted.

Acknowledgement

The research was funded by the National Natural Science Foundation of China (No. 51803170), the Fundamental Research Funds for the Central Universities (No. SWU118125, No. XDJK2020B017 and No. XDJK2018C030), the Entrepreneurship and Innovation Program for Chongqing Overseas Returned Scholars (cx2019050), and the Chongqing Undergraduate Training Program for Innovation and Entrepreneurship (No. S201910635067).

Data availability statement

The data and analysis generated during the study are available from the corresponding author by reasonable request.

References

[1] H.A. Thomason, J.M. Lovett, C.J. Spina, C. Stephenson, A.J. McBain, M.J. Hardman, Silver oxysalts promote cutaneous wound healing independent of infection, Wound Repair and Regeneration: Official Publication of the Wound Healing Society [and] the European Tissue Repair Society 26 (2) (2018) 144–152.
[2] B. Liu, Y. Wang, Y. Miao, X. Zhang, Z. Fan, G. Singh, X. Zhang, K. Xu, B. Li, Z. Hu, M. Xing, Hydrogen bonds autonomously powered gelatin methacrylate hydrogels with super-elasticity, self-heal and underwater self-adhesion for sutureless skin and stomach surgery and E-skin, Biomaterials 171 (2018) 83–96.
[3] A. B. B, V. J, R. B. S, H.M. Khan, A comparative study between conventional skin sutures, staples adhesive skin glue for surgical skin closure, International Surgery Journal 6 (3) (2019) 775.
[4] M.A. Mohamed, M.L. Ahmed, M.G.E. Hagag, M.N.S. Nassar, Stapler versus handswen in small intestinal anastomosis, International Surgery Journal 5 (6) (2018) 2054.
[5] H. Chen, G. Lan, L. Ran, Y. Xiao, K. Yu, B. Lu, F. Dai, D. Wu, F. Lu, A novel wound dressing based on a Konjac glucomannan/silver nanoparticle composite sponge effectively kills bacteria and accelerates wound healing, Carbohydr. Polym. 183 (2018) 70–80.
[6] L. Tang, L. Wen, S. Xu, P. Pi, X. Wen, Ca(2+), redox, and thermoresponsive supramolecular hydrogel with programmed quadruple shape memory effect, Chem. Commun. 54 (58) (2018) 8084–8087.
[7] Y. Zhang, H. Gao, H. Wang, Z. Xu, X. Chen, B. Liu, Y. Shi, Y. Lu, L. Wen, Y. Li, Z. Li, Y. Men, X. Feng, W. Liu, Radiopaque highly stiff and tough shape memory hydrogel microcoils for permanent embolization of arteries, Adv. Funct. Mater. 28 (9) (2018) 1705962.
[8] X. Liu, M. Chang, B. He, L. Meng, X. Wang, R. Sun, J. Ren, F. Kong, A one-pot strategy for preparation of high-strength carboxymethyl xylan-g-poly(acrylic acid) hydrogels with shape memory property, J. Colloid Interface Sci. 538 (2019) 507–518.
[9] Y. Wei, Q. Zeng, M. Wang, J. Huang, X. Guo, L. Wang, Near-infrared light-responsive electrochemical protein imprinting biosensor based on a shape memory conducting hydrogel, Biosens. Bioelectron. 131 (2019) 156–162.
[10] A. Lendlein, R. Langer, Biodegradable, elastic shape-memory polymers for potential biomedical applications, Science 296 (5573) (2002) 1673–1676.
[11] A. Biswas, A.P. Singh, D. Rana, V.K. Aswal, P. Maiti, Biodegradable toughened nanohybrid shape memory polymer for smart biomedical applications, Nanoscale 10 (21) (2018) 9917–9934.
[12] G. Li, Y. Wang, S. Wang, Z. Liu, Z. Liu, J. Jiang, A Thermo- and moisture-responsive zwitterionic shape memory polymer for novel self-healable wound dressing applications, Macromol. Mater. Eng. 304 (3) (2018) 1800603.
[13] S.O. Blacklow, J. Li, B.R. Freedman, M. Zeidi, C. Chen, D.J. Mooney, Bioinspired mechanically active adhesive dressings to accelerate wound closure, Sci. Adv. 5 (7) (2019) eaaw3963.
[14] G. Wu, X. Ma, L. Fan, Y. Gao, H. Deng, Y. Wang, Accelerating dermal wound healing and mitigating excessive scar formation using LBL modified nanofibrous mats, Mater. Des. 185 (2020), 108265.
[15] P. Chuysinuan, N. Chimnoi, N. Reuk-Ngam, P. Khlaychan, A. Makarasen, N. Wetprasit, D. Dechtrirat, P. Supaphol, S. Techasakul, Development of gelatin hydrogel pads incorporated with Eupatorium adenophorum essential oil as antibacterial wound dressing, Polym. Bull. 76 (2) (2018) 701–724.
[16] H. Ur Rehman, Y. Chen, M.S. Hedenqvist, H. Li, W. Xue, Y. Guo, Y. Guo, H. Duan, H. Liu, Self-healing shape memory PUPCL copolymer with high cycle life, Adv. Funct. Mater. 28 (7) (2018), 1704109.
[17] R. Xie, J. Hu, O. Hoffmann, Y. Zhang, F. Ng, T. Qin, X. Guo, Self-fitting shape memory polymer foam inducing bone regeneration: a rabbit femoral defect study, Biochim. Biophys. Acta, Gen. Subj. 1862 (4) (2018) 936–945.
[18] R. Zamani Alavijeh, P. Shokrollahi, J. Barzin, A thermally and water activated shape memory gelatin physical hydrogel, with a gel point above the physiological temperature, for biomedical applications, J. Mater. Chem. B 5 (12) (2017) 2302–2314.
[19] T. Zhu, J. Mao, Y. Cheng, H. Liu, L. Lv, M. Ge, S. Li, J. Huang, Z. Chen, H. Li, L. Yang, Y. Lai, Recent Progress of polysaccharide-based hydrogel interfaces for wound healing and tissue engineering, Adv. Mater. Interfaces 6 (17) (2019), 1900761.
[20] X. He, M. Du, H. Li, T. Zhou, Removal of direct dyes from aqueous solution by oxidized starch cross-linked chitosan/silica hybrid membrane, Int. J. Biol. Macromol. 82 (2016) 174–181.
[21] X. Yang, Y. Chen, S. Yao, J. Qian, H. Guo, X. Cai, Preparation of immobilized lipase on magnetic nanoparticles dialdehyde starch, Carbohydr. Polym. 218 (2019) 324–332.
[22] A.R. Aleem, L. Shahzadi, F. Alvi, A.F. Khan, A.A. Chaudhry, I. ur Rehman, M. Yar, Thyroxin releasing chitosan/collagen based smart hydrogels to stimulate neovascularization, Mater. Des. 133 (2017) 416–425.
[23] R. Pugliese, F. Gelain, Characterization of elastic, thermo-responsive, self-healable supramolecular hydrogel made of self-assembly peptides and guar gum, Mater. Des. 186 (2020), 108370.
[24] C. Cui, T. Wu, F. Gao, C. Fan, Z. Xu, H. Wang, B. Liu, W. Liu, An autolytic high strength instant adhesive hydrogel for emergency self-rescue, Adv. Funct. Mater. 28 (42) (2018), 1804925.
[25] B. Lu, F. Lu, L. Ran, K. Yu, Y. Xiao, Z. Li, F. Dai, D. Wu, G. Lan, Self-assembly of natural protein and imidazole molecules on gold nanoparticles: applications in wound healing against multi-drug resistant bacteria, Int. J. Biol. Macromol. 119 (2018) 505–516.
[26] L.Y. Xia, X. Zhang, M. Cao, Z. Chen, F.G. Wu, Enhanced fluorescence emission and singlet oxygen generation of photosensitizers embedded in injectable hydrogels for imaging-guided photodynamic cancer therapy, Biomacromolecules 18 (10) (2017) 3073–3081.
[27] J. Qu, X. Zhao, Y. Liang, T. Zhang, P.X. Ma, B. Guo, Antibacterial adhesive injectable hydrogels with rapid self-healing, extensibility and compressibility as wound dressing for joints skin wound healing, Biomaterials 183 (2018) 185–199.
[28] S.-H. Lee, S.-R. Shin, D.-S. Lee, Self-healing of cross-linked PU via dual-dynamic covalent bonds of a Schiff base from cystine and vanillin, Mater. Des. 172 (2019), 107774.
[29] J. Joy, J. Pereira, R. Aid-Launais, G. Pavon-Djavid, A.R. Ray, D. Letourneur, A. Meddahi-Pelle, B. Gupta, Gelatin - oxidized carboxymethyl cellulose blend based tubular electrospun scaffold for vascular tissue engineering, Int J Biol Macromol 107(Pt B) (2018) 1922–1935.
[30] A.T. Neffe, B.F. Pierce, G. Tronci, N. Ma, E. Pittermann, T. Gebauer, O. Frank, M. Schossig, X. Xu, B.M. Willie, M. Forner, A. Ellinghaus, J. Lienau, G.N. Duda, A. Lendlein, One step creation of multifunctional 3D architectured hydrogels inducing bone regeneration, Adv. Mater. 27 (10) (2015) 1738–1744.
[31] C. Ghobril, M.W. Grinstaff, The chemistry and engineering of polymeric hydrogel adhesives for wound closure: a tutorial, Chem. Soc. Rev. 44 (7) (2015) 1820–1835.
[32] X. Zhao, H. Wu, B. Guo, R. Dong, Y. Qiu, P.X. Ma, Antibacterial anti-oxidant electroactive injectable hydrogel as self-healing wound dressing with hemostasis and adhesiveness for cutaneous wound healing, Biomaterials 122 (2017) 34–47.
[33] Z. Wei, J.H. Yang, X.J. Du, F. Xu, M. Zrinyi, Y. Osada, F. Li, Y.M. Chen, Dextran-based self-healing hydrogels formed by reversible diels-alder reaction under physiological conditions, Macromol. Rapid Commun. 34 (18) (2013) 1464–1470.
[34] A. Lendlein, S. Kelch, Shape-memory polymers, Angew. Chem. Int. Ed. 41 (12) (2002) 2034–2057.
[35] J. Li, J.A. Viveros, M.H. Wrue, M. Anthamatten, Shape-memory effects in polymer networks containing reversibly associating side-groups, Adv. Mater. 19 (19) (2007) 2851–2855.
[36] J. Huang, L. Zhao, T. Wang, W. Sun, Z. Tong, NIR-triggered rapid shape memory PAM–GO–gelatin hydrogels with high mechanical strength, ACS Appl. Mater. Interfaces 8 (19) (2016) 12384–12392.
[37] A. Suvik, A.W.M. Effendy, The use of modified Masson's trichrome staining in collagen evaluation in wound healing study, J. Neurosurg. 3 (1) (2012) 39–47.
[38] M.H. Flint, M.F. Lyons, M.F. Meaney, D.E. Williams, The Masson staining of collagen — an explanation of an apparent paradox, Histochem. J. 7 (6) (1975) 529–546.
[39] D. Hu, J. Yu, K. Wong, B. Bagchi, P.J. Rossky, P.F. Barbara, Collapse of stiff conjugated polymers with chemical defects into ordered, cylindrical conformations, Nature 405 (6790) (2000) 1030–1033.
[40] V.J. Jones, The use of gauze: will it ever change? Int. Wound J. 3 (2) (2006) 79–88.